Date July 2007
Author Peter Wellens,Jo Pinkster,Arthur Veldman,Rene Huijsmans
Address Delft University of Technology
Ship Hydromechanics Laboratory
Mekelweg 2, 26282 CD Delft

TUDelft

Delft University of Technology

Numerical Wave Run Up Calculations on GBS Columns

by

Peter R Wellens, Jo A. Pinkster, Arthur E.P. Veldman and René H.M. Huijsmans

Report No. 1530-P **2007**

Proceedings of the 7th International Offshore and Polar Engineering Conference, Lisbon, Portugal, July 1-6, 2007, ISBN: 978-1-880653-68-0

Proceedings of the Seventeenth (2007) International Offshore and Polar Engineering Conference
Lisbon, Portugal, July 1-6, 2007

ISBN 978-1-880653-68-5; ISBN 1-880653-68-0(Set); ISSN 1098-6189 (Set)

Numerical Wave Run Up Calculation on GBS Columns

Peter R. Wellens[†], *Jo A. Pinkster*[†], *Arthur E.P. Veldman*[‡], *René H.M. Huijsmans*[†]
[†] Ship Hydromechanics and Structures, Delft University of Technology
Delft, The Netherlands
[‡] Computational Mechanics and Numerical Mathematics, RuG, Groningen, The Netherlands

ABSTRACT

For certain production fields and environments Gravity Based Structures (GBS) are still the preferred type of structure. Critical in the design of a GBS is the deck elevation. If the deck does not rise high enough above the water surface, intolerable wave loading on the sensitive equipment on deck will occur. If the deck is too high, unnecessary costs are involved.

In the past it has been shown that diffraction theory can quite accurately predict wave amplification in direct surroundings of the structure due to the under water caisson. This study will use a combination of diffraction theory and a Navier-Stokes solver with improved Volume Of Fluid method (iVOF) to predict run-up on the columns of a GBS due to the amplified incoming waves. In that case output from diffraction calculations is used as input on the boundaries of the Navier-Stokes domain. In this way waves can enter as well as leave the domain with few reflections. The numerical results for the wave run up on the columns are compared to measurement data.

KEY WORDS: CFD; VOF; diffraction; boundary conditions; run-up;

INTRODUCTION

The designer of production platforms for the sea-based exploitation of oil and gas fields has a number of different types of structure to choose from, either fixed or floating. In a number of circumstances, when the sea, for instance, is not too deep, when the environment is particularly harsh and when storage on site is required, a Gravity Based Structure (GBS) can be the optimal solution for a certain production field. As the name implies, these structures, being composed of concrete in most cases, remain in position by no other means than that they are too heavy to slide away or topple over.

Critical in the design of a GBS is the deck elevation. The criterion for its elevation is that during the GBS's life span the probability of waves impacting the deck is below a certain value. Measurements on site can easily generate enough statistical information about the wave climate to predict the maximum wave height in, say, a thousand or ten-thousand years. But the underwater caisson and the massive cylindrical columns extending through the free surface also have their influence on the waves.

The process of waves being distorted by the presence of a body in the flow is called diffraction. Diffraction can amplify the waves near the structure and when this amplification takes place near a free-surface piercing body, like a column, it is called run-up. This means that information of the wave climate alone cannot lead to a safe deck elevation. In order to assess the impact the presence of a GBS has on the waves, often, model tests are performed.

Model tests, of course, are expensive. During the design process, one might want to evaluate multiple configurations of caisson and columns and the costs of performing model tests for all configurations would be intolerably high. Therefore a need for calculation methods exists that can determine wave amplification in the direct vicinity of the structure. Preferably at lower costs than the experiment.

van Iperen et al. (2004) have shown that linear diffraction theory can quite accurately predict wave amplification due to a GBS. He compared normalized amplitudes, calculated with linear diffraction software, along the center line of the Shell Lunskoye field GBS, to those obtained from experiments. Walker et al. (2006) used second order diffraction theory to predict run-up on the columns of the same structure. Diffraction theory, however, has its limitations: it cannot account for waves overtopping the columns, nor can it deal with energy dissipation due breaking waves.

For a number of years a utility named ComFlow has been under development. ComFlow is based on the non-linear Navier-Stokes equations for an incompressible, viscous fluid, which have been discretized by means of the finite volume method. The free surface is displaced by the Volume Of Fluid (VOF) method and to avoid jetsam and flotsam the VOF method is combined with a local height function. ComFlow's first application was to simulate fluid sloshing in the fuel tank of a satellite and it has been used to simulate blood flow through arteries, wedge entry problems, sloshing in anti-roll tanks and green water loading on ships.

For this paper ComFlow was used to simulate the fluid flow in the direct surroundings of the GBS. This approach also has its drawbacks, because a time-domain simulation requires boundary conditions to introduce waves to the numerical domain. If, at the extremities of the numerical domain, the total wave signal is decomposed in the undisturbed waves and the waves that are diffracted due to presence of the structure, then the boundary conditions will have to manage both the undisturbed and the diffracted wave. At any position along the boundary, waves will have to enter as well as leave the domain with as few reflections as possible.

The traditional approach to boundary conditions in numerical domains is to use damping zones on all sides of the domain that gradually reduce the total wave signal to some specified, undisturbed wave. This requires large domains because the distance over which the damping is built up, is usually as long as the significant wave length encountered during the simulation. The domain can be reduced considerably if the velocities in the fluid at some distance from the structure were known beforehand. For the simulation of the fluid flow around the GBS, the re-

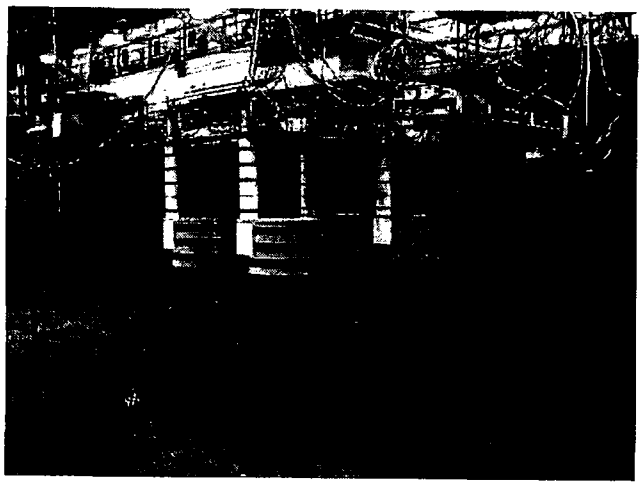

Figure 1: Model of the Lunskoye GBS

sults of a linear diffraction calculation were used to drive the waves in the numerical Navier-Stokes domain. Frequency domain transfer functions for the fluid velocities are Fourier transformed to the time domain and applied as Dirichlet boundary condition for the velocity at every time step. These velocities already comprise the total wave signal: the undisturbed wave is compensated for waves due to the wave diffracting structure.

GOVERNING EQUATIONS COMFLOW

Flow of a homogeneous, incompressible, viscous fluid is described by the continuity equation and the Navier-Stokes equations. The continuity equation describes conservation of mass and the Navier-Stokes equations describe conservation of momentum. In conservative form, they are given by:

$$\oint_{\partial V} u \cdot n dS = 0 \tag{1}$$

$$\int_V \frac{\partial u}{\partial t} dV + \oint_{\partial V} u u^T \cdot n dS = -\frac{1}{\rho} \oint_{\partial V} (pn - \mu \nabla u \cdot n)\, dS + \int_V F dV \tag{2}$$

Here, ∂V is the boundary of volume V, $u = (u, v, w)$ is the velocity vector in the three coordinate directions, n is the normal of volume V, ρ denotes the density, p is the pressure, ∇ is the gradient operator. Further μ denotes the dynamic viscosity and $F = (Fx, Fy, Fz)$ is an external body force, for example gravity.

Boundary conditions

At the solid walls of the computational domain and at the objects inside the domain, a no-slip boundary condition is used. This condition is described by $u = 0$ for fixed boundaries, and $u = u_b$ for moving objects with u_b the object velocity. Some of the domain boundaries may let fluid flow in or out of the domain. Especially, when performing wave simulations, an inflow boundary is needed where the incoming wave is prescribed and at the opposite boundary a non-reflecting outflow condition should be used. When using the domain decomposition, the velocities at the boundaries of the COMFLOW domain are prescribed using the wave kinematics calculated by the far field solver.

Free surface

If the position of the free surface is given by $s(x,t) = 0$, the displacement of the free surface is described using the following equation:

$$\frac{Ds}{Dt} = \frac{\partial s}{\partial t} + (u \cdot \nabla)\, s = 0 \tag{3}$$

At the free surface, boundary conditions are necessary for the pressure and the velocities. Continuity of normal and tangential stresses leads to the equations:

$$-p + 2\mu \frac{\partial u_n}{\partial n} = -p_0 + 2\gamma H \mu \left(\frac{\partial u_n}{\partial t} + \frac{\partial u_t}{\partial n} \right) \tag{4}$$

Here, u_n is the normal component of the velocity, p_0 is the atmospheric pressure, γ is the surface tension and $2H$ denotes the total curvature.

NUMERICAL MODEL IN COMFLOW

To solve the Navier-Stokes equations numerically, the computational domain is covered with a fixed Cartesian grid. The variables are staggered, which means that the velocities are defined at cell faces, whereas the pressure is defined in cell centers. The body geometry is piecewise linear and cuts through the fixed rectangular grid. Volume apertures (F^b) and edge apertures (A_x, A_y, and A_z) are used to indicate for each cell which part of the cell and cell face respectively is open for fluid and which part is blocked by solid geometry. To track the free surface, the volume-of-fluid function F_s is used, which is 0 if no fluid is present in the cell, 1 if the cell is completely filled with fluid and between 0 and 1 if the cell is partly filled with fluid. The Navier-Stokes equations are solved in every cell containing fluid. Cell labeling is introduced to distinguish between cells of different characters. First the cells which are completely blocked by geometry are called B(oundary) cells. These cells have volume aperture $F_b = 0$. Then the cells which are empty, but have the possibility of letting fluid flow in are labeled E(mpty). The adjacent cells, containing fluid, are S(urface) cells. The remaining cells are labeled as F(luid) cells. Note that these cells do not have to be completely filled with fluid. In Figure 2 an example of the labeling is given.

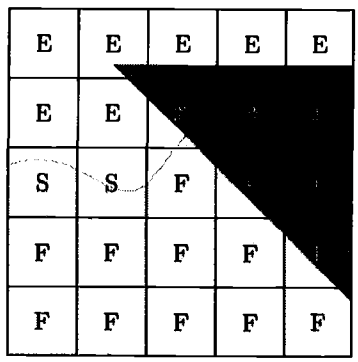

Figure 2: Cell labeling: dark gray represents the body, light gray the fluid

Discretisation of the continuity equation

The continuity and Navier-Stokes equations are discretised using the finite volume method. The natural form of the equations when using the

finite volume method is the conservative formulation as given in Eq. (1) and (2). In this paper, the discretisation is explained in two dimensions. In most situations, this can be extended to three dimensions in a straightforward manner.

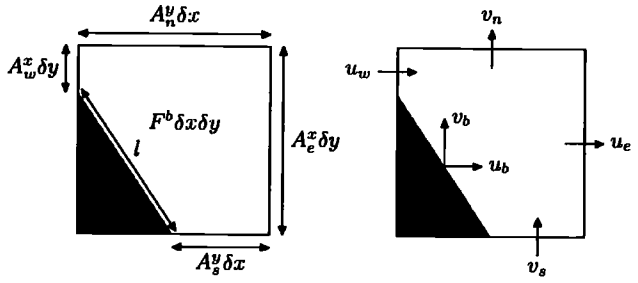

Figure 3: Conservation cell for the continuity equation.

In Figure 3 a computational cell is shown, which is cut by the body geometry. When applying conservation of mass in this cell, the discretisation results in

$$u_e A_e^x \delta y + v_n A_n^y \delta x - u_w A_w^x \delta y - v_s A_s^y \delta x + u_b \left(A_e^x - A_w^x\right) \delta y + v_b \left(A_n^y - A_s^y\right) \delta x = 0 \quad (5)$$

where the notation is explained in Figure 3.

Discretisation of the momentum equations

The momentum equations are discretised in a control volume with the velocity as center. In Figure 4 the control volume is drawn for the x-momentum equation for an open cell (left) and a cell that is partly cut by the geometry (right). All the terms of the Navier-Stokes equations are discretised in these control volumes using the finite volume method. The discretisations of the different terms are explained in (Kleefsman et al. 2005).

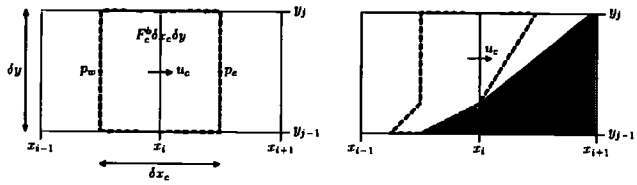

Figure 4: A control volume for the discretisation of the Navier-Stokes equation in x-direction in the case of an uncut cell (left) and a cut cell (right).

subsectionTemporal discretisation and solution method The continuity and Navier-Stokes equations are discretised in time using the forward Euler method. This first order method is accurate enough, because the order of the overall accuracy is already determined by the first order accuracy of the free surface displacement algorithm. Using superscript n for the time level, the temporal discretisation results in

$$M^0 u_h^{n+1} = -M^b u_b^{n+1} \quad (6)$$

$$\Omega \frac{u_h^{n+1} - u_h^n}{\delta t} = -C\left(u_h^n, u_b\right) u_h^n - \frac{1}{\rho}\left(\left(M^0\right)^T p_h^{n+1} - \mu D u_h^n\right) + F_h^n \quad (7)$$

The continuity equation is discretised at the new time level to ensure a divergence free velocity field. The spatial discretisation is written in matrix notation where M is the divergence operator with M^0 working on the interior velocities and M^b on the boundary velocities, Ω contains cell volumes, C contains the convection coefficients (which depend on the velocity vector) and D contains diffusive coefficients. To solve the system of equations, the equations are rearranged to:

$$u_h^{n+1} = \tilde{u}_h^n + \delta t \Omega^{-1} \frac{1}{\rho} \left(M^0\right)^T p_h^{n+1} \quad (8)$$

where

$$\tilde{u}_h^n = u_h^n - \delta t \Omega^{-1} \left(C\left(u_h^n\right) u_h^n - \frac{\mu}{\rho} D u_h^n - F_h^n\right) \quad (9)$$

First, an auxiliary vector field $\tilde{u}_h^n$ is calculated using Eq. (9). Next, Eq. (8) is substituted in Eq. (6) which results in a Poisson equation for the pressure. From this equation the pressure is solved using the SOR (Successive Over Relaxation) method where the optimal relaxation parameter is determined during the iterations. Once the pressure field is known, the new velocity field is calculated from $\tilde{u}_h^n$ using the pressure gradient.

HANDLING OF THE FREE SURFACE

After the new velocity field has been calculated, the free surface can be displaced. This is done using an adapted version of the volume-of-fluid method first introduced by Hirt and Nichols (1981). A piecewise constant reconstruction of the free surface is used, where the free surface is displaced by changing the VOF value in a cell using calculated fluxes through cell faces. The original VOF method has two main drawbacks. The first is that flotsam and jetsam can appear, which are small droplets disconnecting from the free surface (Rider and Kothe 1998). The other drawback is the gain or loss of water due to rounding of the VOF function. By combining the VOF method with a local height function (Kleefsman et al. 2005), these problems do not appear any more. The local height function is adopted in the following way. For every surface cell, locally a height function is defined, which gives the height of the water in a column of three cells as in Figure 5. The direction in which the function is defined is the direction of the coordinate axis that is most normal to the free surface. Then not the individual fluxes of the three cells are updated, but the height function is updated using fluxes through the boundaries of the column of the three cells (the dashed-lined region in Figure 5). The individual VOF values of the three cells are then calculated from the height of the water in the column. When using this adopted fluid displacement algorithm, the method is strictly mass conservative and almost no flotsam and jetsam appear.

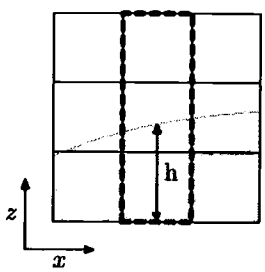

Figure 5: The VOF function in cells near surface cells is updated using a local height function.

MOVING OBJECTS IN COMFLOW

In the domain an object, which moves according to a prescribed or calculated motion, can be present. Every time step the object is moved, so new geometry apertures for the cell volumes F^b and the cell edges A^x, A^y have to be calculated. This calculation must be as accurate as possible, because this has a large influence on the smoothness of the pressure field. When the apertures are not calculated exactly, the object seems to be breathing in time, which causes irregularities in the pressure signal. In two dimensions, the apertures can be calculated almost exactly. In Fekken (2004) a procedure has been explained how to do this. When using an exact calculation of apertures in three dimensions, cross-sections of polyhedrons with the rectangular grid are needed, which can not be determined in a very straightforward manner. Therefore, in three dimensions a more simple method is adopted, which approximates the three-dimensional body geometry. The general procedure can be described in three steps. First, the starting geometry is stored in a special way using markers. Then, every time step the volume apertures are calculated by moving the markers. Finally, the edge apertures are calculated, based on the volume apertures. At the start of a simulation, the geometry is built from the finite element description given by the user. To calculate the volume and edge apertures, the object is filled with a subgrid of markers. For every cell the number of markers of the cell inside the object is counted, determining the part of the cell that is occupied by an object. If a moving object is present in the domain, the geometry of the object should be stored, such that it can be displaced every time step. Therefore, the markers inside a moving object are stored in an array. Around each marker, a small rectangular volume is defined, such that the union of all the volumes forms the object. To prevent unnecessary storage, the markers in a computational cell that is completely solid will be replaced by one marker with accompanying volume equal to the volume of the computational cell. During the simulation the volume and edge apertures in the computational grid change every time step. New volume apertures must be calculated with the use of the markers and volumes defined at the start of the simulation. First, the markers are moved according to the motion of the rigid object. In case of a rotation of the object, also the volumes belonging to the marker cells should be rotated. To calculate volume apertures, the cross-sections of the marker volumes with the computational cells should be calculated. For a general rotated volume, this is very complicated in three dimensions. To avoid the calculation of these difficult cross-sections, the marker volumes are not rotated, but are staying grid aligned as in the right of Figure 6. The errors introduced by keeping the volumes grid aligned, namely small holes or small overlapping regions, are not very large.

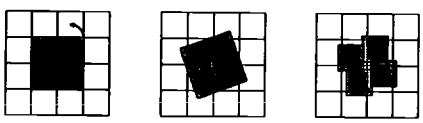

Figure 6: Rotation of a square: starting situation (left); exact rotation (middle); rotation where the marker volumes are kept grid aligned (right).

After the volume apertures have been calculated at the start of every time step, the edge apertures must be determined. The edge apertures are calculated using a piecewise linear reconstruction of the geometry. This method is often used for the reconstruction of the interface between two fluids, as explained in (Rider and Kothe 1998). First, in every cell the normal of the body is calculated based on the filling ratios of adjacent cells. Using this, a linear approximation of the body geometry in the cell is created where the filling ratio of the cell is needed. The edge apertures are determined by the fractions of the cell faces that are cut by the linear approximation. In (Fekken 2004) it has been shown that the edge apertures calculated in this way behave smoothly in time.

EXPERIMENTAL DATA

A number of model tests with different sea states and for several deck elevations were performed at the CHC facility in Canada. Of these tests only the regular tests with the characteristics mentioned in Table 1 were used. The deck was elevated to its topmost position to prevent any possible impact with the waves.

Type	Wave Height [m]	Period [s]
regular	14	12.7
regular	10	12.7

Table 1: Experiment characteristics.

As can be seen from Figure 1 the structure consists of a box shaped under-water caisson with four large diameter concrete columns extending from the caisson through the water surface. The caisson measures 120m by 110m and is 15m high. The columns are 26m in diameter where they intersect with the caisson and 24m in diameter at mid-height. They are spaced 68m apart in front-to-back direction and 40m apart in the side-to-side direction. Because the water depth during the experiments was 53m and the columns were 45m tall, they extend about 7m above the mean surface level. Steel columns are mounted to the concrete substructure to eventually carry the deck. The positions of the wave run-up probes during the experiments are shown in Figure 7. Waves travel in the positive x-direction.

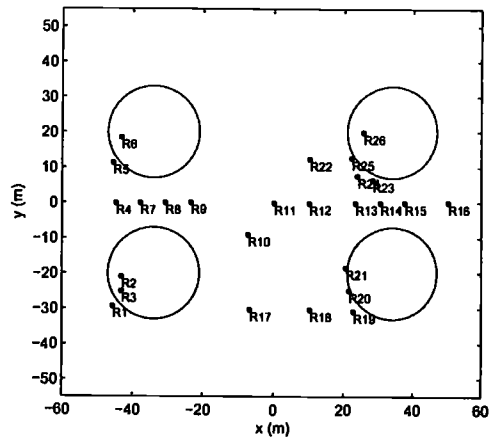

Figure 7: The layout of the concrete substructure and the positions of the wave run-up probes

LINEAR DIFFRACTION

The diffraction calculations were performed using standard 3D linear radiation-diffraction software in the frequency domain. Figure 8 shows the panel model that was used to perform the calculation; it consists of around 2000 panels for one fourth of the total structure.
The surface elevation η is obtained from:

$$\eta = -\frac{1}{g}\frac{\partial \Phi}{\partial t} \tag{10}$$

In Eq. 10 Φ is the total potential, which consists of the undisturbed and the diffracted potential:

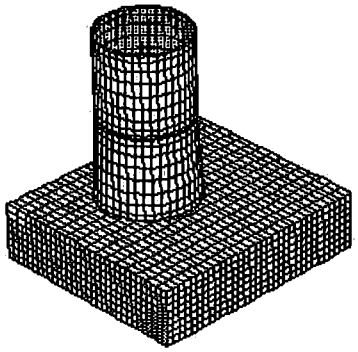

Figure 8: Panel model of the GBS

$$\Phi = \phi_0 + \phi_d \tag{11}$$

The diffracted potential, in turn, comes from:

$$\phi_d(x,y,z) = \frac{1}{4\pi}\iint_{S_0} \sigma(\hat{x},\hat{y},\hat{z})G(x,y,z,\hat{x},\hat{y},\hat{z})dS_0 \tag{12}$$

where σ is the initially unknown source strength, S_0 is the mean wetted area of the body, G is the Green's function, which satisfies the Laplace equation, the linearized boundary conditions at the free surface and the sea bed, and the radiation condition to infinity. The velocities in each direction follow from the derivatives of the total potential in that direction, $(u,v,w)^T = \nabla\Phi$. In Figure 9 the transfer functions for the surface elevation obtained from linear diffraction along the center line of the structure are compared to the normalized amplitudes from the measured regular wave tests with both $H = 10m$ and $H = 14m$.
Along the center line there is a fairly good agreement between the calculated transfer functions and the measurements. The shift in $-x$-direction of the minimum in front of the first columns has already been addressed in (van Iperen et al. 2004). No explanation for this shift was found. Behind the latter columns the difference between the calculated and the measured normalized amplitudes increases. This could be the result of local energy dissipation due to wave breaking.

BOUNDARY CONDITION

To investigate the phenomena of the shift of minimum and the disagreement between the measured and calculated results beyond $x = 40m$, a more detailed simulation was required. Because the overall match between the diffraction results and the measurements was quite good, the diffraction results in terms of velocities were used to drive a fully nonlinear simulation with ComFlow. The velocities obtained from diffraction are used as Dirichlet boundary condition for the velocity. In this way a local boundary condition is created that introduces the undisturbed waves to the ComFlow domain while compensating for the outgoing, diffracted waves. The required number of grid cells for the numerical simulation at the same resolution can be smaller because no numerical damping zones have to be present.

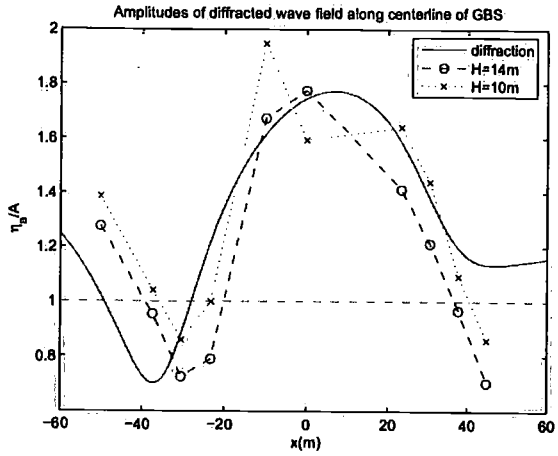

Figure 9: Transfer functions of the surface elevation along the center line of the structure compared to normalized amplitudes from the experiments

The frequency domain results are Fourier transformed to the time domain. The simulation starts from a fully developed flow field at $t = 0$ with the velocities and surface elevations obtained from transformed linear diffraction results. The velocities at the boundaries are updated at every consecutive time step. Because velocities in linear diffraction are only defined up to the mean surface, an engineering approach called Wheeler stretching is used to determine the velocities up to the actual free surface. With Wheeler stretching the vertical coordinate is transformed by means of the following relation:

$$z = \frac{z' - h(q-1)}{q} \text{ where } q = \frac{h}{h+\eta} \tag{13}$$

In Eq. 13 h is the mean water depth and η is the elevation of the actual surface above $z = 0$. In this way all vertical coordinates are stretched towards the actual free surface.

RESULTS COMFLOW SIMULATION

The numerical simulation was performed on a grid consisting of 500,000 cells with a resolution of about $(dx, dy, dz) = (1, 1, 1)$. Some stretching was applied in the vertical direction, where the grid was the most dense around the mean surface. The initial condition at $t = 0s$ consists of the surface elevations and the Wheeler stretched velocities from the diffraction calculation. The simulation was for regular waves with wave height $H = 14m$ and period $T = 12.7s$. Two periods were simulated taking about three hours computational time on a regular desktop with a 3GHz processor. Figure 10 shows the flow at consecutive time instances. Several stages can be observed: the wave builds up as it passes the structure and overtops the concrete columns on the downstream side of the structure.

The results of the simulation for the wave probes along the center line are compared to the results from the experiments. In Figure 11 a graph similar to the one in Figure 9 is shown. One can see that the normalized amplitudes from the simulation are quite close to the ones obtained from the experiment.

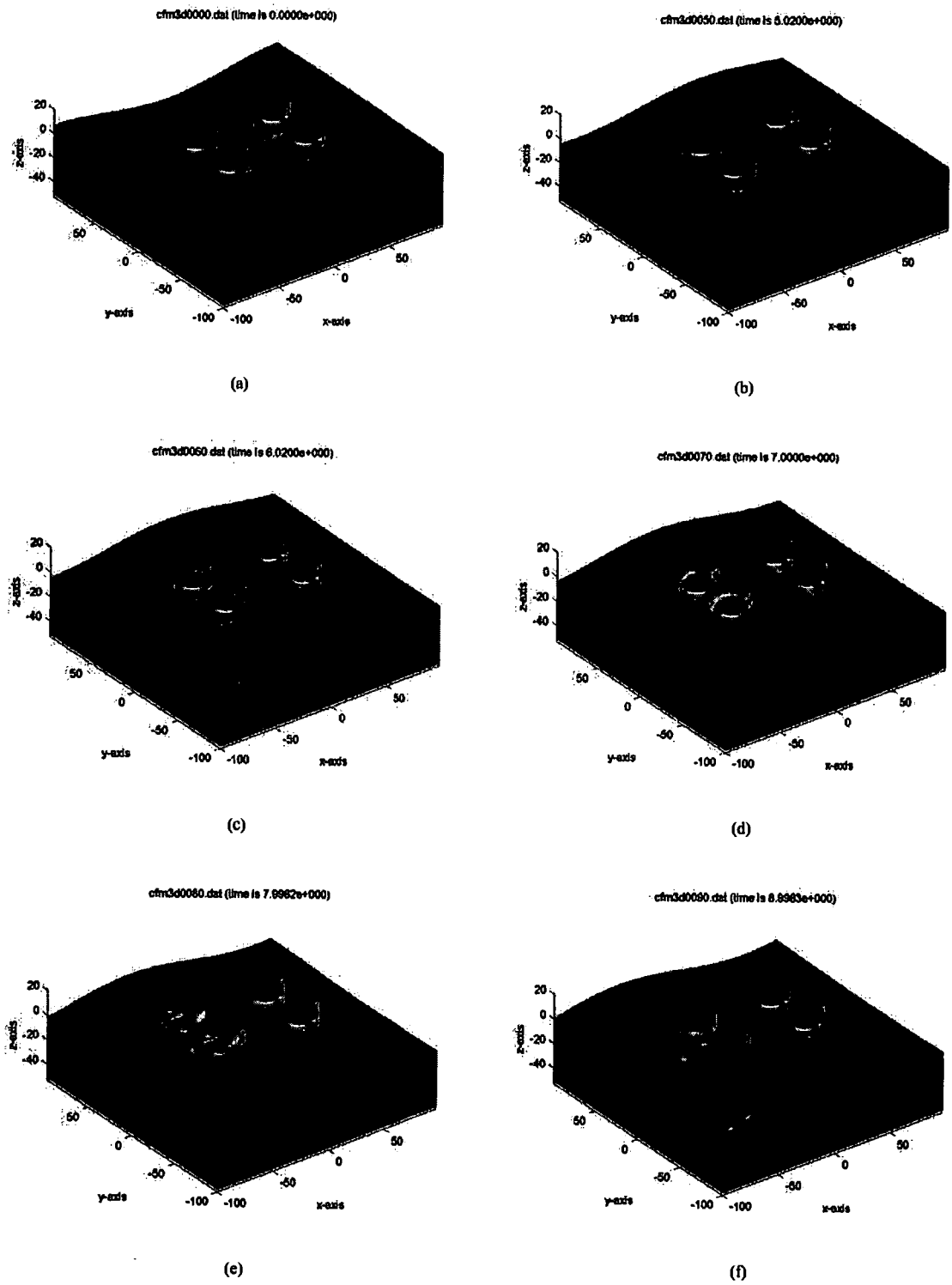

Figure 10: Snapshots of the simulation at different time instances.

The surface elevation near the columns was compared to both the experimental data and the diffraction results. The normalized amplitudes are summarized in Table 2. Diffraction overestimates the run-up on the columns as can be expected: the structure is modeled up to the mean surface and no overtopping of fluid can be accounted for. The simulation compares nicely to the experiments.

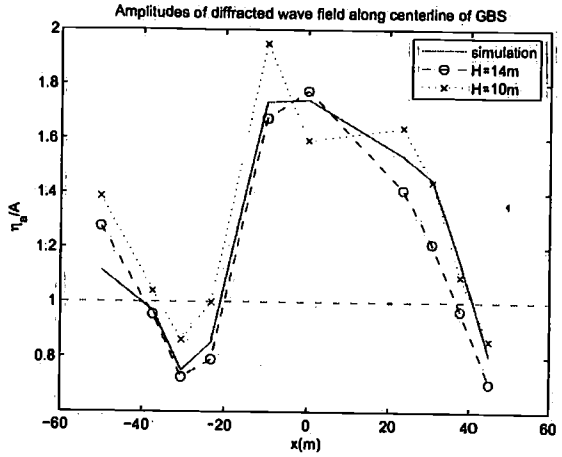

Figure 11: Simulated normalized amplitudes of the surface elevation along the center line of the structure compared to normalized amplitudes from the experiments

Probe	Simulation	Diffraction	Experiment
R1	0.84	0.89	1.09
R5	0.95	0.92	1.16
R21	1.40	1.34	1.56
R25	1.05	1.11	1.27

Table 2: Normalized amplitudes of the surface elevation near the columns

CONCLUSION AND DISCUSSION

In this paper it was shown that linear diffraction results, in terms of surface elevations and velocities, can be used to drive a fully non-linear Volume Of Fluid simulation. The initial condition for the simulation is composed entirely of the velocities and surface elevations from linear diffraction. At every consecutive time step only the velocities and the surface elevations at the boundaries of the domain are updated.

Linear diffraction by itself already gives a reasonable estimate of the surface elevations near the structure, but it cannot account for wave breaking and overtopping of the columns. It was shown that a VOF simulation of the flow in the direct surroundings of the GBS has a better agreement with the experiment than linear diffraction.

A significant reduction of computational time can be obtained by combining linear diffraction results and a VOF simulation. This is due to the fact that no numerical damping zones are required to account for the outgoing waves. Numerical damping zones are usually at least one wavelength long. The linear diffraction based boundary condition is a local boundary condition that introduces waves to the numerical domain while, at the same time, compensating for the outgoing waves. In addition, the simulation does not have to be started with the fluid at rest. It would take one or two periods to gradually build up the simulation to the desired wave height. Starting with a fully developed flow field, instead, also saves a considerable amount of computational time.

Nonetheless, some remarks have to be made. The linear solution at $t = 0$ is not the exact solution. Because it is forced upon the domain at the start of the simulation, some spurious waves will be introduced. These waves will fully reflect back into the domain when they reach the boundaries, since they are not included in the linear diffraction results. In this case, with a GBS in regular waves, the spurious waves are small.

The Wheeler stretching procedure, furthermore, is not a transformation technique with a sound physical background. By Wheeler stretching the velocities to the actual free surface some errors in the form of spurious waves will be introduced to the domain, which again will not be dealt with at the boundaries. All in all this means that if the simulation will go on for long enough, at one point the spurious waves will start to dominate the solution and unrealistic results will be obtained.

At this point in the development of Computational Fluid Dynamics (CFD), where we have to restrict ourselves to simulating snapshot events in restricted domains because of computer time and memory, the linear diffraction type boundary condition agrees well with our needs. When simulations will be performed in larger domains and for longer periods of time, then more accurate boundary conditions will be necessary.

ACKNOWLEDGEMENTS

The authors would like to thank Shell International Exploration and Production, Rijswijk, for providing the experiment data used in this paper. This research is supported by the Dutch Technology Foundation STW, applied science division of NWO and the technology programme of the Ministry of Economic Affairs.

References

Fekken, G. (2004, March). *Numerical simulation of free surface flow with moving objects*. Ph. D. thesis, University of Groningen.

Hirt, C. W. and B. D. Nichols (1981). Volume of fluid (vof) method for the dynamics of free boundaries. *Journal Of Computational Physics 39*(1), 201–225.

Kleefsman, K. M. T., G. Fekken, A. E. P. Veldman, B. Iwanowski, and B. Buchner (2005, June). A volume-of-fluid based simulation method for wave impact problems. *Journal Of Computational Physics 206*(1), 363–393.

Rider, W. J. and D. B. Kothe (1998, April). Reconstructing volume tracking. *Journal Of Computational Physics 141*(2), 112–152.

van Iperen, E. J., G. Z. Forristall, J. A. Battjes, and J. A. Pinkster (2004, August). Amplification of waves by a concrete gravity substructure: Linear diffraction analysis and estimating the extreme crest height. *Journal Of Offshore Mechanics And Arctic Engineering-Transactions Of The Asme 128*(3), 211–223.

Walker, D. A. G., P. H. Taylor, R. E. Taylor, and J. Zang (2006). Diffraction theory as a tool for predicting airgap beneath a multi-column gravity based structure. *Proceedings Of The Sixteenth (2006) International Offshore And Polar Engineering Conference 3*(1), 165–172.